

AD-A250 398



92-13138



CONDITIONS OF RELEASE

0124144

310269

MR PAUL A ROBEY  
DTIC  
Attn:DTIC-FDAC  
Cameron Station-Bldg 5  
Alexandria  
VA 22304 6145  
USA

\*\*\*\*\*

DRIC U

COPYRIGHT (c)  
1988  
CONTROLLER  
HMSO LONDON

\*\*\*\*\*

DRIC Y

Reports quoted are not necessarily available to members of the public or to commercial organisations.

**DEFENCE RESEARCH AGENCY**

**Aerospace Division**

**RAE Pyestock**

Technical Memorandum P 1223

Received for printing 24 February 1992

Accession For	
NTIS GRA&I	<input checked="" type="checkbox"/>
DTIC TAB	<input type="checkbox"/>
Unannounced	<input type="checkbox"/>
Justification	
By	
Distribution/	
Availability Codes	
Dist	Avail and/or Special
A-1	

**MEASUREMENTS AND COMPUTATIONS OF EXTERNAL HEAT  
TRANSFER AND FILM COOLING IN TURBINES**

by

S. P. Harasgama

C. D. Burton

K. S. Chana

**SUMMARY**

A review of recent work on turbine heat transfer performed at the RAE (Pyestock) is presented. The work covers the effects of secondary flows on turbine nozzle guide vane heat transfer with and without film cooling. It is shown that the heat load to the platforms (endwalls) are significantly affected by the secondary flow action. The platform film cooling data has been well correlated with flat plate single row film cooling data to within  $\pm 11\%$ . A three-dimensional Navier-Stokes computational study of the effects of turbine inlet temperature distortion on the thermo-fluid mechanics within a rotating blade passage is given. It is shown that the temperature distortion is modified within the rotor blade and can lead to increased pressure side and over tip heat transfer.

*A paper presented at the tenth International Symposium On Air Breathing Engines (ISABE) 1-6 September 1991, Nottingham, UK.*

Copyright  
©  
Controller HMSO London  
1992

**LIST OF CONTENTS**

	<b>Page</b>
INTRODUCTION	3
TEST FACILITY	4
TURBINE STATOR HEAT TRANSFER RESULTS	4
TURBINE STATOR FILM COOLING RESULTS	6
HOT GAS MIGRATION WITHIN ROTOR BLADES	8
CONCLUSIONS AND OBSERVATIONS	9
Acknowledgments	10
References	10
Illustrations	Figures 1-19
Report documentation page	inside back cover

## MEASUREMENTS AND COMPUTATIONS OF EXTERNAL HEAT TRANSFER AND FILM COOLING IN TURBINES

S.P. Harasgama, C.D. Burton & K.S. Chana  
Royal Aerospace Establishment  
Propulsion Department, Pyestock,  
Farnborough, Hampshire, U.K.

### ABSTRACT

A review of recent work on turbine heat transfer performed at the RAE (Pyestock) is presented. The work covers the effects of secondary flows on turbine nozzle guide vane heat transfer with and without film cooling. It is shown that the heat load to the platforms (endwalls) are significantly affected by the secondary flow action. The platform film cooling data has been well correlated with flat plate single row film cooling data to within  $\pm 11\%$ . A Three-Dimensional Navier-Stokes computational study of the effects of turbine inlet temperature distortion on the thermo-fluid mechanics within a rotating blade passage is given. It is shown that the temperature distortion is modified within the rotor blade and can lead to increased pressure side and over tip heat transfer.

### NOMENCLATURE

A	Film cooling superposition parameter
B	Film cooling superposition parameter
-B/A	Cooling Effectiveness
$C_t$	Vane tangential chord
d	Cooling hole diameter
G	Blowing rate ( $\Gamma_i U_i / \Gamma_g U_g$ )
h	Heat transfer coefficient
I	Momentum flux ratio ( $\Gamma_i U_i^2 / \Gamma_g U_g^2$ )
k	Thermal conductivity of air
M	Mach number
Nu	Nusselt number
Q	Heat Flux
Re	Reynolds number
S	Streamwise dimension
S2	Pitchwise dimension
T	Temperature
U	Velocity
X	Axial dimension
$\rho$	Density
$\theta$	Temp. Diff. Ratio $(T_g - T_i) / (T_g - T_w)$
$\phi$	Cooling function parameter

### Subscripts

cp	Corrected for property variations
g	Gas path value
i	Injectant value
o	Datum (uncooled) value
t	Total (stagnation) value
w	Wall value

### INTRODUCTION

Turbine heat transfer research has been undertaken at the RAE in both experimental and computational fields. In the main, the work has concentrated on the heat transfer resulting from the three-dimensional (3D) nature of the flow field within high pressure turbine stators and rotors. These secondary flows have been well catalogued in terms of their aerodynamic impact<sup>1,2</sup>. The endwall inlet boundary layers give rise to two sets of secondary flows. The passage vortex is caused by overturning of the endwall boundary layers within the turbine passage. In addition, a horse-shoe vortex is formed by the stagnation of the endwall boundary layers at the blade leading edge. Both mechanisms cause a migration of flow towards the suction side of the passage and can lead to increased losses.

Heat transfer studies on the effects of secondary flow have also been reported by several authors<sup>3-7</sup>. It is shown that the horse shoe vortex has a major effect on the platform heat transfer and also on the vane suction side. The horse shoe vortex strips off the incoming boundary layer and this gives rise to a new boundary layer starting just downstream of the separation line. This results in enhancing the heat load in the downstream region.

The heat transfer effects due to radial variations in inlet temperature are brought about by hot streaks generated within the combustor and is essentially an unsteady effect<sup>13</sup>. Early analytical work<sup>14</sup> has indicated that density stratification in a rotating passage can give rise to secondary flows due to Coriolis and Centripetal accelerations affecting the flow. Recent two-dimensional viscous numerical simulations<sup>15,16</sup> show that the hot gas is transported within the blade passage and is deposited onto the blade pressure side. Viscous 3D computations<sup>17,18</sup> additionally show that hot gas migrates radially leading to enhanced rotor tip heat transfer.

This paper reviews the work done at the RAE on experimental and computational heat transfer in turbines. Detailed results of heat transfer on a fully annular geometry

of the aerofoils and platforms of turbine nozzle guide vanes along with flow visualisations which corroborate the heat transfer distributions are presented. Full coverage film cooling data on the endwall of a high pressure vane are also presented and correlated with axial pressure gradient. A computational study using a fully 3D Navier Stokes code<sup>8</sup> on the effects of combustor generated temperature distortion within a rotating turbine blade passage is also reviewed.

#### TEST FACILITY

The Isentropic Light Piston Cascade (ILPC) as shown in Figure 1 is derived from the short duration thermo-fluids facilities pioneered at Oxford University<sup>9</sup>. The facility operates by rapidly compressing air with a light piston which raises its pressure and temperature to a required level. Subsequently a fast acting valve is opened and the air is discharged over the set of turbine vanes/blades. The compression time of the facility is 1.0sec with a run time of 0.5sec when operating at a gas-to-wall temperature ratio of 1.5. Engine similarity conditions of Reynolds number and Mach number prevail for the 0.5sec run time. For film cooling studies, a mixture of air and carbon-dioxide ( $CO_2$ ) was used to obtain the correct coolant-to-gas density ratio whilst maintaining the correct gas-to-wall temperature ratio.

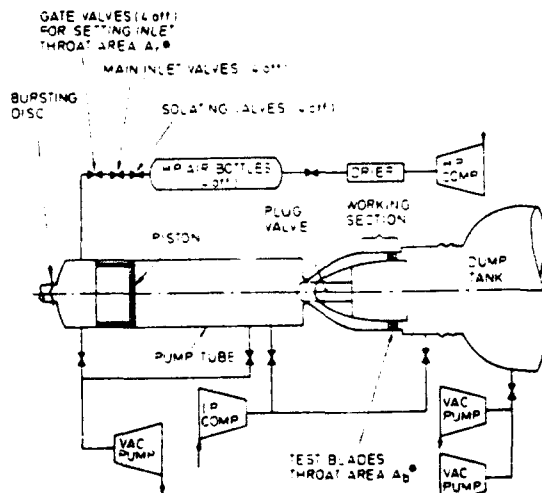


Fig 1 ILPC Test Facility

The vanes under test are manufactured from machineable glass ceramic (MACOR<sup>®</sup>) which has a low thermal diffusivity. Thin film heat transfer gauges are deposited onto the surface of the vanes and monitor the temperature during the run time. The heat transfer coefficients are obtained by solving the one-dimensional transient heat conduction equation. A vane with typical instrumentation and platform film cooling holes is shown on Figure 2. A sufficient

number of thin-film gauges were placed on the vanes to give accurate measurements of the heat transfer distributions. In all cases aerodynamic data were acquired at the same locations as the heat transfer measurements. This was achieved by having static pressure tappings on the vanes and



Fig 2 Heat Transfer & Cooling Blade

total pressure probes upstream of the turbine module. The inlet free stream turbulence intensity was set to around 6% by a bar grid placed 4.5 chords upstream of the cascade.

#### TURBINE STATOR HEAT TRANSFER RESULTS

The heat transfer to the aerofoils suction surface is shown on Figure 3. The Nusselt number (Nu) contours indicate the extent of three-dimensionality of the heat loads. For all Reynolds numbers and Mach numbers the secondary flow has transported low energy endwall boundary layer flow onto the suction surface. These boundary layers are relatively thick and thereby reduce the root and tip heat transfer rates. The flow visualisation of Figure 4 tends to corroborate the heat transfer patterns. It can be seen that flow migrating across the suction surface appears to come from the endwall boundary layers.

Platform Nusselt number contours are shown on Figure 5. The heat transfer patterns are significantly non-uniform and this again is attributed to the horse-shoe vortex and the passage secondary flow. It can be seen that as the Reynolds number is increased the high heat transfer region migrates across the endwall and moves upstream. A similar effect is observed as the Mach number is increased. In all cases the increase in Reynolds number results in an increase of Nusselt number as expected. This trend is the opposite for increasing Mach number. The high heat transfer rates in the downstream portion of the passage are caused by the horse shoe vortex which strips off the incoming boundary layer and causes a thin new, high energy, boundary layer to form.

The flow visualisation of Figure 6 shows the nature of the secondary flow on the

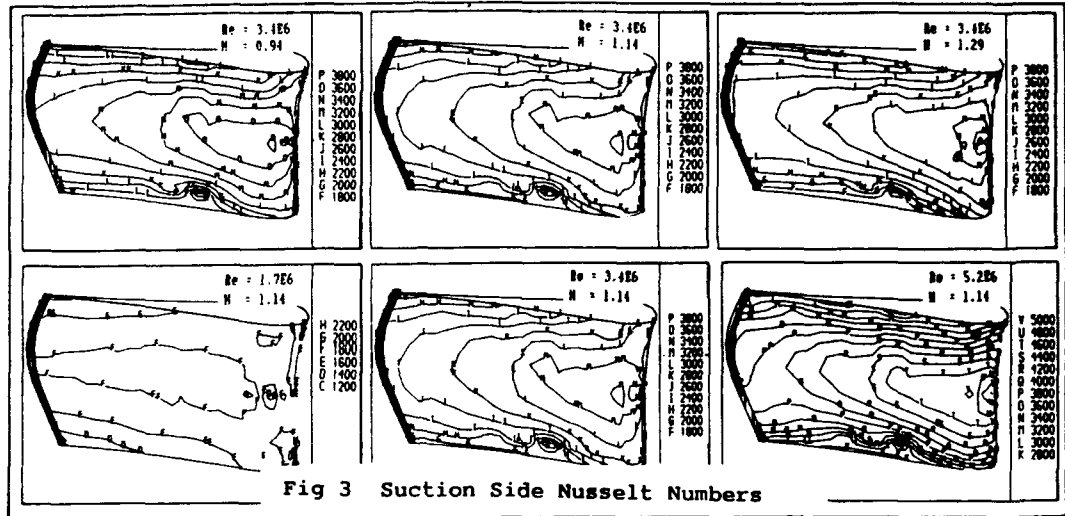


Fig 3 Suction Side Nusselt Numbers



Fig 4 Suction Side Flow Vis.

vane platform. The horse shoe vortex can be clearly seen to start just upstream of the leading edge and traverse across the passage until it meets the suction surface at around 40% axial chord. A computation was performed with the 3D Navier Stokes code to predict the secondary flow field and this is shown on Figure 7. The code was run with 25 radial, 83 axial and 25 blade-to-blade grid points with an inlet boundary layer thickness of approximately 5% annulus height on both endwalls. Computations were performed with the code in the fully turbulent mode throughout. It can be seen that the agreement between prediction and experiment is qualitatively very good. These predictions yield further insight into the nature of the secondary flows and corroborate the heat transfer results.

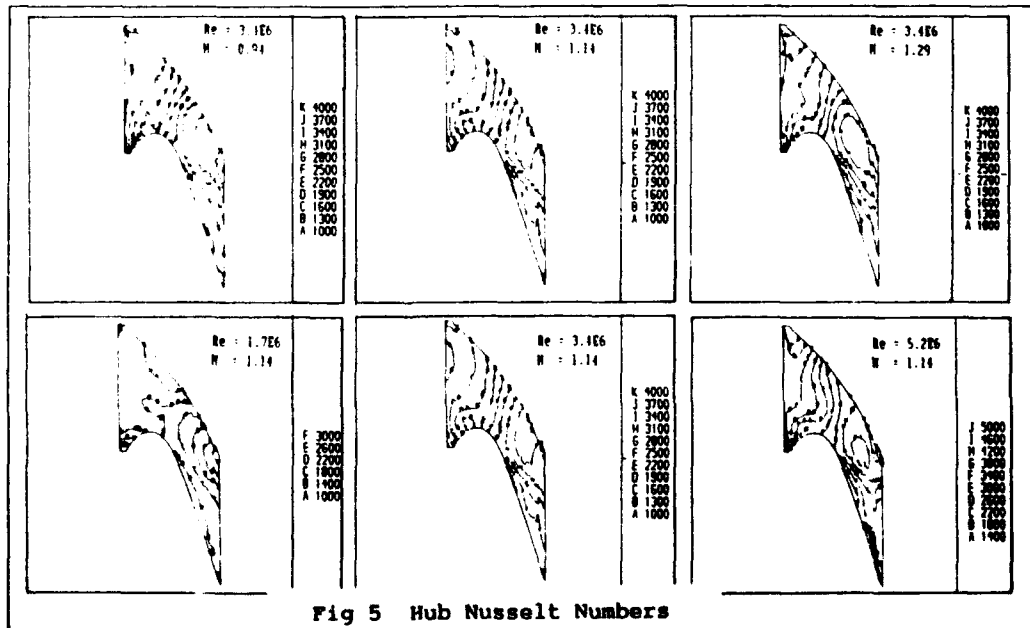


Fig 5 Hub Nusselt Numbers

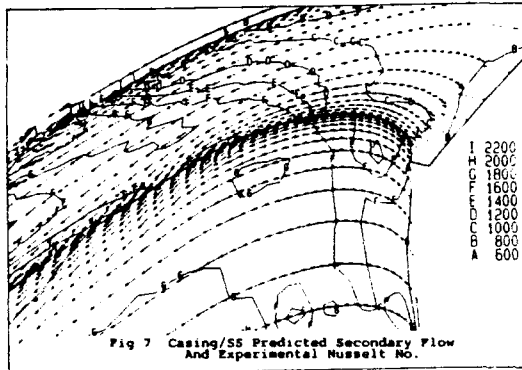


Fig 7 Casing/SS Predicted Secondary Flow And Experimental Nusselt No.

#### TURBINE STATOR FILM COOLING RESULTS

Experimental data on film cooling tests within a fully annular turbine stator vane passage are reported. The tests were done on the outer platform of the vane. These tests were performed to corroborate a design philosophy of placing cooling holes on an iso-Mach line. Such a design will generate a uniform blowing rate across the whole passage. Consider the Momentum Flux Ratio :

$$I = (\Gamma_i * U_i^2) / (\Gamma_g * U_g^2) \quad 1$$

$$I = (P_{ti} - P_i) / (P_{tg} - P_g) \quad 2$$

In the turbine situation the free stream and cooling total pressures are fixed by compressor exit conditions, as is the cooling static pressure. Hence the only variable is  $P_g$ , which is constant along an iso-Mach line. Placing the film cooling holes along such a line will yield a constant momentum flux ratio, which for a fixed density ratio yields a uniform blowing rate ( $G$ ).

For the present tests the vane Reynolds number was set to approximately  $2.6 \times 10^6$  based on exit conditions and tangential chord. The Exit Mach number was 0.93 and the gas-to-wall temperature ratio ( $T_g/T_w$ ) was 1.30. The engine cooling design required a density ratio of 1.8 and a temperature difference ratio ( $\theta$ ) of 1.75.

In order to achieve these conditions a heavy gas, carbon-dioxide, was mixed with air to simulate density ratio's up to 2.0. The coolant was injected using a separate reservoir with a fast acting valve which fed a plenum just below the surface of the platforms being cooled. The coolant was injected synchronously with the onset of main stream flow.

The Nusselt number contours on the cooled platform are shown on Figure 8. These data are for increasing blowing rate ( $G$ ) from 0.53 to 1.11 for a fixed  $\theta$  of 1.62, also shown is the datum (uncooled) result. It can be seen that as  $G$  is increased the Nusselt numbers decrease significantly. Figure 9 shows a similar Nusselt number pattern for  $G = 1.11$  and  $\theta$  increasing from 0.87 to 1.62. Here again  $Nu$  decreases with increasing  $\theta$ . In both figures it is clear that the suction side of the platform is receiving more cooling than the pressure side. This is because the secondary flow convects the coolant towards the suction side which is evident from the flow visualisation of Figure 6. Figure 10 shows the ratio of cooled-to-uncooled Nusselt numbers for  $G = 1.11$  &  $\theta = 1.44$ , it is clear that over most of the platform the heat load is reduced by 75% whilst at the pressure side corner the reduction is about 20%.

These data have been analysed using the superposition approach<sup>10</sup> to film cooling. All data have been normalised to constant property conditions<sup>11</sup> using:

$$(Nu/Nu_0)_{cp} = (Nu/Nu_0) * (T_w/T_g)^n \quad 3$$

The superposition representation is:

$$(Nu/Nu_0)_{cp} = A + B\theta \quad 4$$

Where  $n = -0.25$  for a turbulent boundary layer.  $A$  and  $B$  are constants of proportionality in the superposition formulation<sup>12</sup>.

Figure 11 shows the linearity of the energy equation when applied to these data and indicates that the superposition formulation holds even in the presence of strong secondary flows. This enables the present data to be extrapolated to other engine operating conditions. Also shown are the platform cooling effectiveness on Figure 12a&b. Figure 12a shows the streamwise variation of effectiveness which indicates that there is a gradual reduction of  $-B/A$  in the downstream direction as the coolant mixes with the mainstream gas. It also indicates a reduction of  $-B/A$  from suction to pressure side which is more explicitly presented in Figure 12b. This indicates that the suction side effectiveness is greater than the pressure side value for any axial distance due to secondary flow effects.

The present data have been successfully correlated with single row film cooling results on a flat plate with zero axial

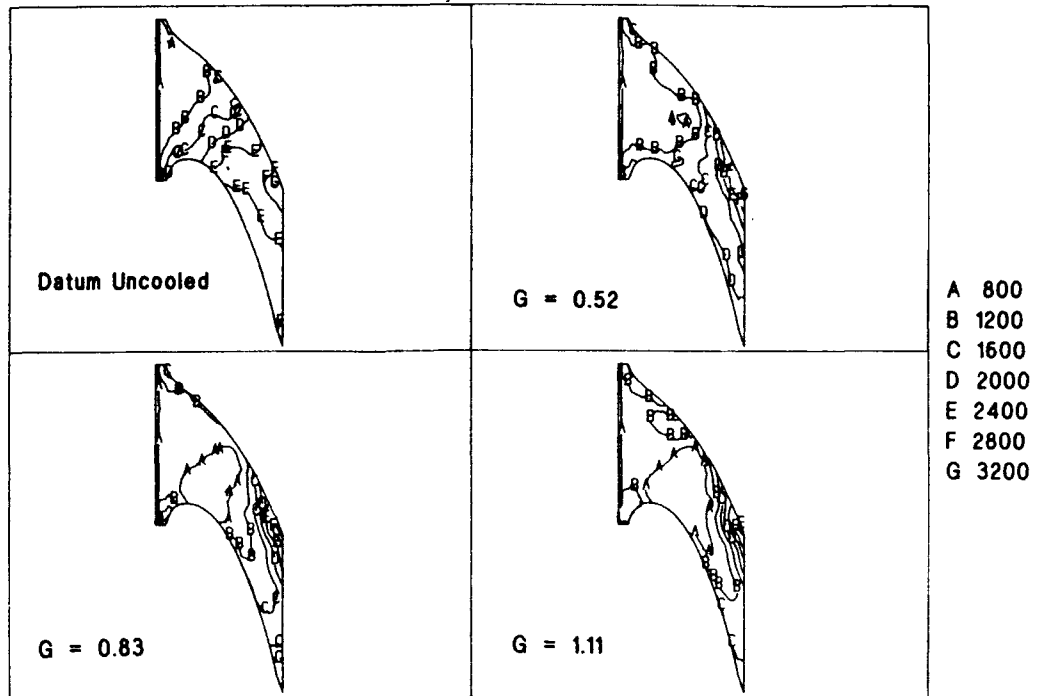


Fig 8 Casing Nusselt Numbers for  $\theta=1.62$ , All G

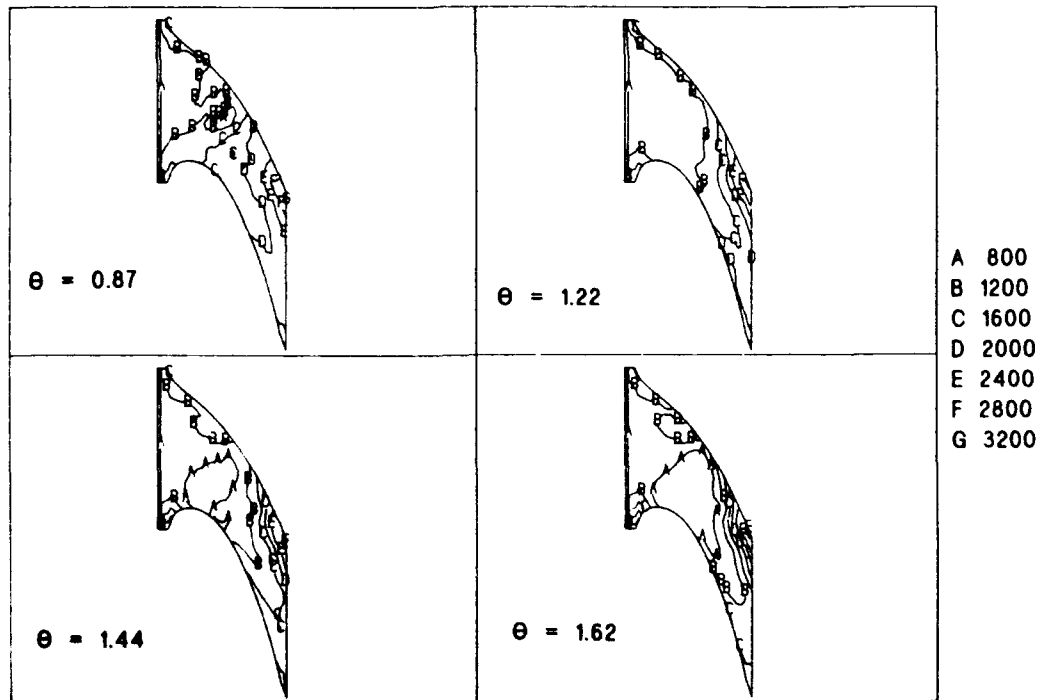


Fig 9 Casing Nusselt Numbers for  $G=1.11$ , All  $\theta$

\* MACOR - Trademark of Corning, U.S.A

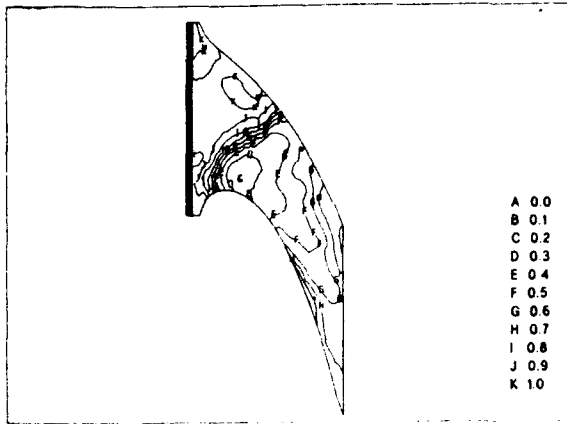


Fig 10 Ratio of Cooled To Uncooled Nusselt Number For C = 1.11 &  $\theta = 1.44$

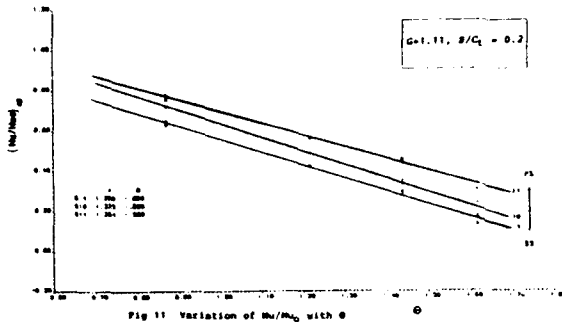


Fig 11 Variation of  $Nu/Nu_0$  with  $\theta$

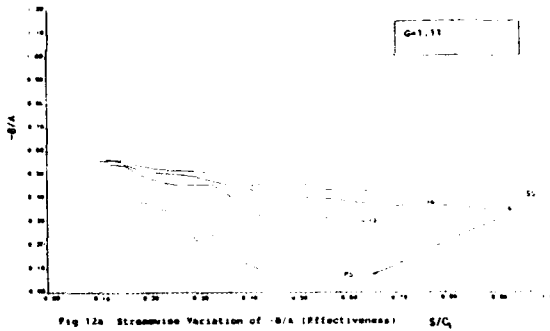


Fig 12a Streamwise Variation of  $\theta/A$  (Effectiveness)  $S/C_t$

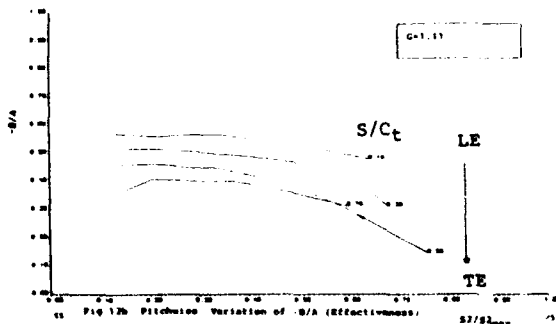


Fig 12b Pitchwise Variation of  $\theta/A$  (Effectiveness)  $S/C_{t_{max}}$

pressure gradient. This was achieved by modifying the present data with a correction for the turbine pressure gradient. It has been shown<sup>12</sup> that the ratio  $Nu/Nu_0$  can be put as:

$$(Nu/Nu_0)_{cp} = \Phi(S/d) \times (U_i/U_g)^{-4/3} \quad 5$$

A modification was made to the present data by multiplying it by  $(U/U_{inlet})^{0.2}$  and plotting against Equation 5. The value  $n=0.2$  was chosen by arguing that, usually, heat transfer coefficients can be put as functions of Reynolds number (velocity) raised to the power 1/5th or 4/5th. The results of this analysis are shown on Figure 13a&b. Figure 13a shows the data plotted against the discrete single row injection parameter (Eq-5). It is seen that  $(Nu/Nu_0)_{cp}$  lies below the flat plate zero pressure gradient correlation. The corrected data are shown on Figure 13b. It can be seen that Equation 5 now represents the platform data very well. The scatter about the line is only  $\pm 11\%$ , which is considered to be very good in the present case of large secondary flows.

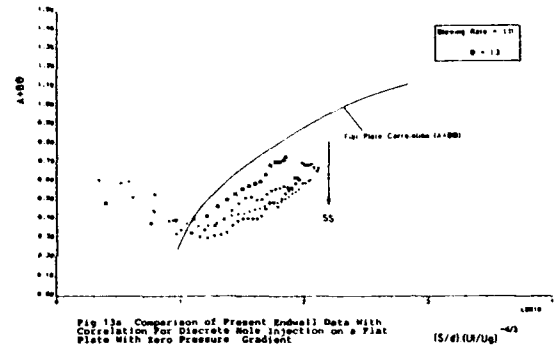


Fig 13a Comparison of Present Endell Data With Correlation For Discrete Hole Injection on a Flat Plate With Zero Pressure Gradient

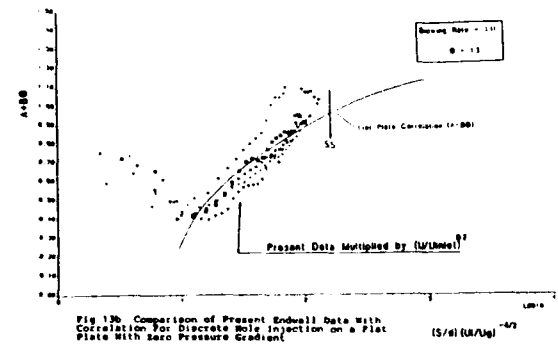


Fig 13b Comparison of Present Endell Data With Correlation For Discrete Hole Injection on a Flat Plate With Zero Pressure Gradient

**HOT GAS MIGRATION WITHIN ROTOR BLADES**

The effect of inlet temperature distortion on the thermo-fluid mechanics in the rotor blade has been computed<sup>17</sup> using a steady state three-dimensional Navier-Stokes code<sup>8</sup>. The inlet temperature distortion is generated by the combustor burners and affects the rotor blading as they pass through these hot patches; it is therefore an unsteady effect. However, an "average" effect of the hot gas migration can be

evaluated using a steady state 3D viscous computation in order to gain an understanding of the flow physics.

The simulation of inlet temperature distortion was achieved with a parabolic radial temperature profile as shown on Figure 14. The computational grid for the rotor blade is shown on Figure 15. The 3D Navier-Stokes code<sup>8</sup> was run with 67-axial, 25-radial and 25-blade-to-blade grid points. The predicted secondary flow

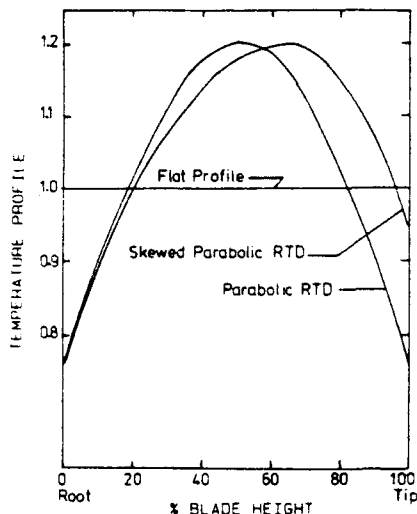


Fig 14 Inlet Radial Temperature

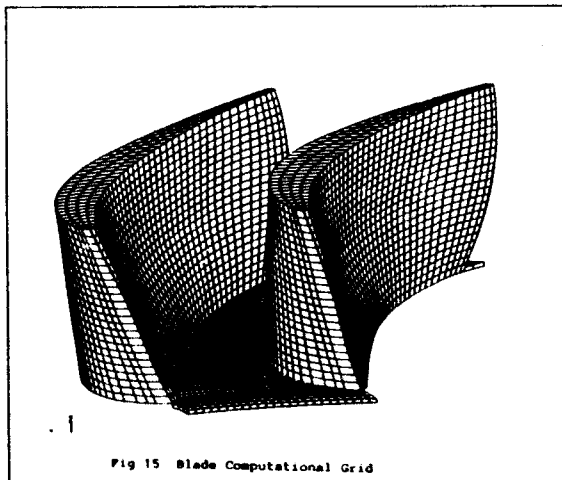


Fig 15 Blade Computational Grid

patterns are given on Figure 16. It can be seen that the computations with radial temperature distortion give higher secondary flows. Figure 17 shows the over tip Mach number distributions which reach a peak value of 1.80 and this will also enhance the rotor tip heat transfer rates.

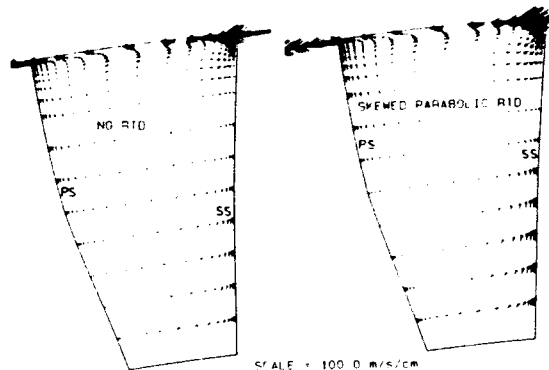


Figure 16 Secondary Flow Vectors at 30% Axial Chord

Contours of rotor relative total temperature are given in Figure 18. This shows that the hot gas migrates from the mid-span region at turbine inlet to the pressure side tip of the blade by 80% axial chord. The hot gas subsequently enters the tip gap and is entrained into the tip vortex. The heat transfer enhancement on the blade pressure side due to hot gas migration is shown on Figure 19. This indicates a 75% enhancement due to hot gas migration. The actual increase will be periodic and fluctuate between 0% and 75% as the blade passes through the hot gas patches.

#### CONCLUSIONS & OBSERVATIONS

Full three-dimensional heat transfer distributions have been measured on turbine vanes operating at engine representative conditions. The effects of secondary flow on heat transfer are large. Rotor blade heat transfer is significantly affected by inlet temperature distortion. The main conclusions are as follows:

- The secondary flow reduces the root and tip heat transfer on the vane suction side due to low energy endwall fluid migrating from the endwall regions.
- Endwall heat transfer is also affected by secondary flow leading to high heat transfer near the pressure side trailing edge.
- Flow visualisations indicate that the horse-shoe vortex sweeps off the incoming endwall boundary layer. This leads to high energy free stream gas forming a thin new boundary layer, giving high heat transfer.
- Platform film cooling data indicate good effectiveness when the injectant emerges into a uniform pressure field. This data has been successfully correlated to  $\pm 11\%$  of flat plate results.

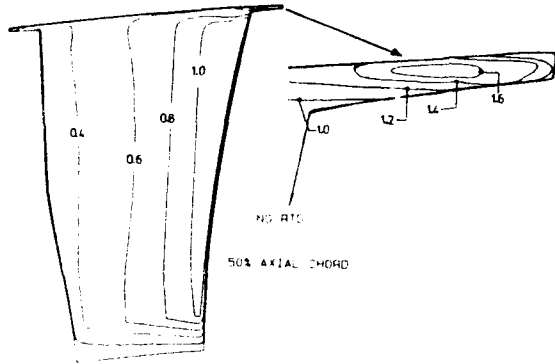


Figure 17 Mach Numbers In Tip Gap, Axial View

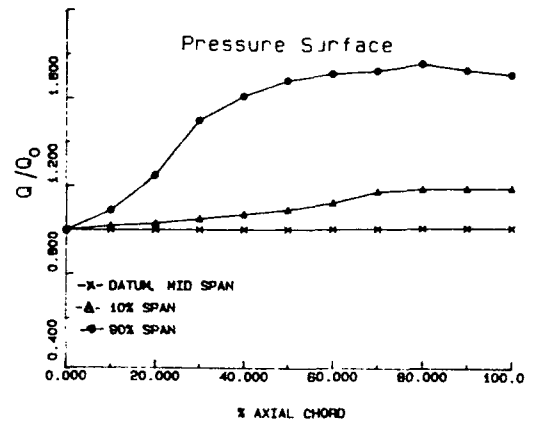


Fig 19 Ratio of Heat Flux With RTD To Without RTD

- Rotor blade pressure side heat transfer is increased due to hot gas migration. The maximum increase can reach 75% as the blades pass periodically through hot gas patches generated by the combustor.

**ACKNOWLEDGEMENTS**

Thanks are due to Mr K.J. Walton who maintained the test facility. The turbomachinery heat transfer group at Oxford University led by Professor Terry Jones were instrumental in launching the RAE effort, their invaluable advice and encouragement are gratefully acknowledged.

**REFERENCES**

1. Langston L.S., Nice M.L. & Hooper R.M. (1977), "Three-dimensional flow within a turbine blade passage", ASME Jnl. of Eng. for Gas Turbines & Power, Vol-99, pp21-28.  
 2. Sieverding C.H. (1985), "Recent progress in the understanding of basic aspects of secondary flows in turbine blade passages" ASME Jnl of Engineering for Gas Turbines and Power, April, Vol-107, pp248-257.

3. Gaugler R.E. & Russell L.M. (1983), "Comparison of visualised turbine endwall secondary flows and measured heat transfer patterns". NASA Tech. Memo. TM83016.

4. Boyle R.J. & Russell L.M. (1989), "Experimental determination of stator endwall heat transfer". ASME Paper Number:89-GT-219.

5. Wedlake E.T., Brooks A. & Haragama S.P. (1989), "Aerodynamic and heat transfer measurements on a transonic nozzle guide vane", Trans. ASME, Jnl. of Turbomachinery Vol 111, pp36-42.

6. Haragama S.P. & Wedlake E.T. (1990) "Heat transfer and aerodynamics of a high rim speed turbine nozzle guide vane tested in the RAE Isentropic Light Piston Cascade (ILPC)". ASME Paper Number:90-GT-41, to be published in ASME Jnl. of Turbomachinery.

7. Jones T.V., Harvey N.W., Ireland P.T. & Wang Z (1989) "Detailed heat transfer measurements in nozzle guide vane passages in linear and annular cascades in the presence of secondary flows". AGARD-CP-422

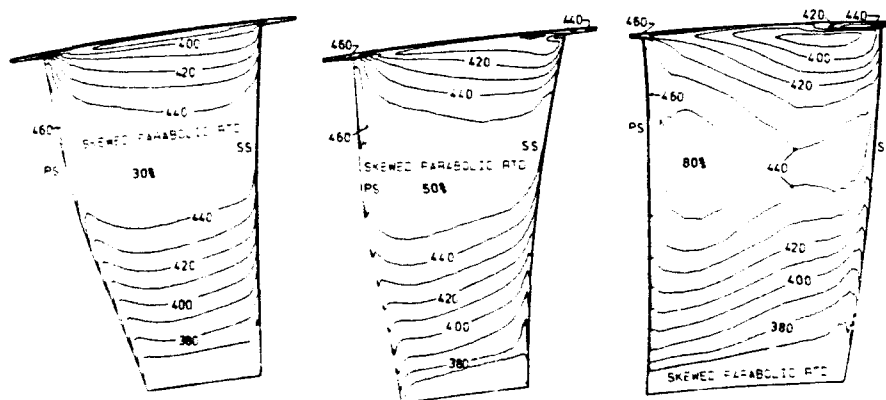


Figure 18 Total Temperature Contours

8. Dawes W.N. (1986). "A numerical method for the analysis of 3D viscous compressible flow in turbine cascades; Application to secondary flow development in a cascade with and without dihedral", ASME paper number: 86-GT-145

9. Schultz D.L. & Jones T.V. (1973), "On the flow in an isentropic light piston tunnel". ARC, R&M-3731.

10. Metzger D.E., Carper H.J. & Swank L.R. (1968), "Heat transfer with film cooling near non-tangential injection slots", ASME Jnl. of Eng. for Power, April.

11. Jones T.V., Forth C.J.P., Fitt A.D. & Robertson B.A. (1986), "Temperature ratio effects in compressible boundary layers", Int. Jnl. of Heat & Mass Transfer, Vol 29

12. Jones T.V. (1986), "The scaling of film cooling, theoretical & experimental results", VKI-LS-1986-06.

13. Butler T.L., Sharma O.P., Joslyn H.D. & Dring R.P. (1986), "Redistribution of an inlet temperature distortion in an axial flow turbine". AIAA Paper: AIAA-86-1468.

14. Hawthorne W.R. (1974), "Secondary vorticity in stratified compressible fluids in rotating systems", Univ. of Cambridge, CUED/A-TURBO/TR63.

15. Rai M.M & Dring R.P. (1987), "Navier-Stokes analyses of the redistribution of inlet temperature distortion in a turbine" AIAA Paper: AIAA-87-2146.

16. Krouten B. & Giles M.B. (1988), "Numerical investigation of hot streaks in turbines". AIAA Paper: AIAA-88-3015.

17. Harasgama S.P. (1990), "Combustor exit temperature distortion effects on heat transfer and aerodynamics within a rotating turbine blade passage", ASME No:90-GT-174

18. Sharma O.P., Pickett G.F & Ni R.H. (1990), "Assessment of unsteady flows in turbines", ASME Paper No: 90-GT-150

## GENERAL INSTRUCTIONS FOR COMPLETING SF 298

The Report Documentation Page (RDP) is used in announcing and cataloging reports. It is important that this information be consistent with the rest of the report, particularly the cover and title page. Instructions for filling in each block of the form follow. It is important to *stay within the lines* to meet *optical scanning requirements*.

**Block 1. Agency Use Only (Leave blank).**

**Block 2. Report Date.** Full publication date including day, month, and year, if available (e.g. 1 Jan 88). Must cite at least the year.

**Block 3. Type of Report and Dates Covered.** State whether report is interim, final, etc. If applicable, enter inclusive report dates (e.g. 10 Jun 87 - 30 Jun 88).

**Block 4. Title and Subtitle.** A title is taken from the part of the report that provides the most meaningful and complete information. When a report is prepared in more than one volume, repeat the primary title, add volume number, and include subtitle for the specific volume. On classified documents enter the title classification in parentheses.

**Block 5. Funding Numbers.** To include contract and grant numbers; may include program element number(s), project number(s), task number(s), and work unit number(s). Use the following labels:

C - Contract	PR - Project
G - Grant	TA - Task
PE - Program Element	WU - Work Unit Accession No.

**Block 6. Author(s).** Name(s) of person(s) responsible for writing the report, performing the research, or credited with the content of the report. If editor or compiler, this should follow the name(s).

**Block 7. Performing Organization Name(s) and Address(es).** Self-explanatory.

**Block 8. Performing Organization Report Number.** Enter the unique alphanumeric report number(s) assigned by the organization performing the report.

**Block 9. Sponsoring/Monitoring Agency Name(s) and Address(es).** Self-explanatory.

**Block 10. Sponsoring/Monitoring Agency Report Number.** (If known)

**Block 11. Supplementary Notes.** Enter information not included elsewhere such as: Prepared in cooperation with...; Trans. of...; To be published in.... When a report is revised, include a statement whether the new report supersedes or supplements the older report.

**Block 12a. Distribution/Availability Statement.** Denotes public availability or limitations. Cite any availability to the public. Enter additional limitations or special markings in all capitals (e.g. NOFORN, REL, ITAR).

DOD - See DoDD 5230.24, "Distribution Statements on Technical Documents."

DOE - See authorities.

NASA - See Handbook NHB 2200.2.

NTIS - Leave blank.

**Block 12b. Distribution Code.**

DOD - Leave blank.

DOE - Enter DOE distribution categories from the Standard Distribution for Unclassified Scientific and Technical Reports.

NASA - Leave blank.

NTIS - Leave blank.

**Block 13. Abstract.** Include a brief (*Maximum 200 words*) factual summary of the most significant information contained in the report.

**Block 14. Subject Terms.** Keywords or phrases identifying major subjects in the report.

**Block 15. Number of Pages.** Enter the total number of pages.

**Block 16. Price Code.** Enter appropriate price code (*NTIS only*).

**Blocks 17. - 19. Security Classifications.** Self-explanatory. Enter U.S. Security Classification in accordance with U.S. Security Regulations (i.e., UNCLASSIFIED). If form contains classified information, stamp classification on the top and bottom of the page.

**Block 20. Limitation of Abstract.** This block must be completed to assign a limitation to the abstract. Enter either UL (unlimited) or SAR (same as report). An entry in this block is necessary if the abstract is to be limited. If blank, the abstract is assumed to be unlimited.